Laser-diode interferometer with a photothermal modulation

Takamasa Suzuki, Mineki Matsuda, Osami Sasaki, and Takeo Maruyama

A laser-diode (LD) interferometer that uses an accurate photothermal-modulating technique is proposed. Since this technique with the photothermal method modulates only a wavelength of the LD, measurement accuracy is not affected by an intensity modulation that usually appears in the current modulation. The fundamental characteristics of this technique are investigated in detail. The new setup is tested, and its accuracy is compared with that of a previous system. © 1999 Optical Society of America

OCIS codes: 120.3180, 120.3930, 120.5050, 120.5060, 140.2020, 140.6810.

1. Introduction

We can modulate the wavelength of the laser diode (LD) by changing the injection current, a feature that is commonly used in the construction of a variety of interferometers. This technique is called the current modulation (*C* modulation). Unfortunately, the injection current affects not only the wavelength but also the optical power of the LD, which in turn affects the measurement accuracy.

A heterodyne LD interferometer[1] and a phase-shifting LD interferometer[2] use triangular and stepwise injection current, respectively, to modulate the wavelength of the LD. In such interferometers the intensity modulation that is introduced by the optical power change in the LD, the so-called intensity modulation, always occurs. This undesired change has to be normalized by a numerical calculation[2] or by an electrical circuit.[3] Measurement error caused by the intensity modulation in a phase-shifting LD interferometer has also been analyzed theoretically.[4] A sinusoidal phase-modulating LD interferometer uses sinusoidal injection current.[5] Although the interferometer does not require large phase shift and although the amplitude of the injection current is small, the detected interference signal contains slight errors caused by the power change in the LD.

A two-wavelength LD interferometer that is insensitive to the LD's optical power change[6] has been proposed. In this interferometer, phases in the two interferograms are shifted in opposite directions to each other by use of the stepwise injection current. Since the amplitude of one interference signal increases, while the another decreases, the intensity changes caused by the modulating current cancel each other in the sum of these two interference signals. If a single LD is used, however, this technique cannot be used to eliminate the influence of the optical power change in the LD. In such a case the intensity-compensating processes mentioned above are necessary.

Another technique, however, which uses what is called the photothermal effect, in which a high-power laser beam is directed at the active region of a second LD, is proposed[7] and analyzed.[8] The change of the optical power is dramatically reduced in this photothermal modulation (*P* modulation). But suppressing the change of the optical power is not an ideal technique, since laser-chip temperature variations affect optical output power even when the driving current is constant.

Our technique effectively unites the two methods described above; whereas the latter is used to modulate the LD, the former functions as a means of compensating for photothermal modulation-induced changes in optical power. With this two-pronged approach the current and the photothermal modulation (*CP* modulation) enable us to use a purely phase-modulated laser beam. Therefore the compensating process for the intensity modulation is no longer necessary in the signal processing.

The modulating characteristics of both *P* and *CP* modulation are investigated in detail. We estimate measurement errors caused by the optical power

The authors are with the Faculty of Engineering, Niigata University, 8050 Ikarashi 2, Niigata 950-2181, Japan. T. Suzuki's e-mail address is takamasa@eng.niigata-u.ac.jp.

Received 26 May 1999; revised manuscript received 9 August 1999.

0003-6935/99/347069-07$15.00/0

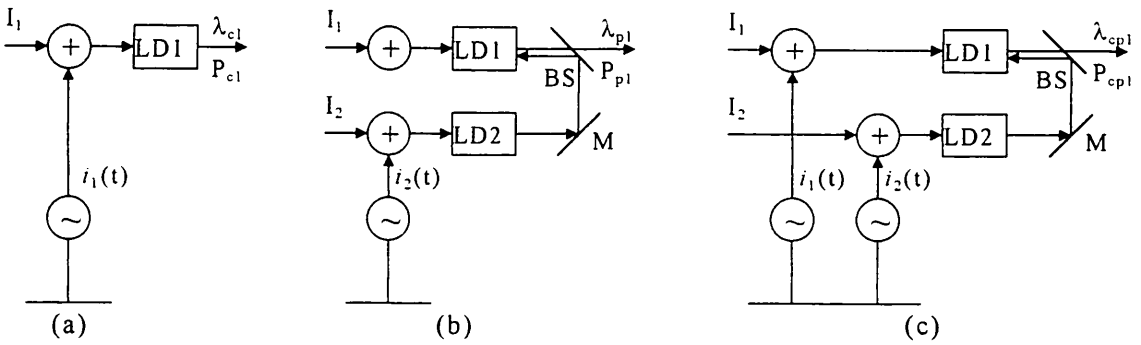

Fig. 1. Schematic of (a) *C* modulation, (b) *P* modulation, and (c) *CP* modulation. BS, beam splitter; I, dc bias current; LD1, laser for a light source; LD2, heating laser; M, mirror.

change in the LD by means of surface-profile measurements with *C*, *P*, and *CP* modulation.

2. Principle

A. Current Modulation

Schematics of *C*, *P*, and *CP* modulation are shown in Fig. 1. A LD's wavelength and optical power vary according to the amount of injection current supplied, as shown in Fig. 2, because the cavity length of the LD changes according to the heat generated by the injection current.[3] The *C* modulation illustrated in Fig. 1(a), which uses the tunability of the LD's wavelength shown in Fig. 2(a), simplifies realization of wavelength modulation and is widely used in interferometers. At this point, however, undesirable change occurs in the optical power as shown in Fig. 2(b). When both dc bias current I_1 and modulating current

$$i_1(t) = a_1 \cos(\omega_m t + \theta_1) \tag{1}$$

are injected into LD1 as shown in Fig. 1(a), the wavelength varies by

$$\lambda_{c1}(t) = [\Delta\lambda_{c1}/\Delta i_1] i_1(t) \equiv \beta_1 i_1(t) \tag{2}$$

around the central wavelength λ_0, where subscript 1 means that the variable is mainly related to LD1. At the same time the optical power changes by

$$P_{c1}(t) = [\Delta P_{c1}/\Delta i_1] i_1(t) \equiv \gamma_1 i_1(t), \tag{3}$$

where β_1 and γ_1 are LD1's modulating efficiency and coefficient of the optical power change, respectively, that are illustrated in Fig. 2. The square brackets enclosing this parameter indicate the gradient of the line in Fig. 2 or Fig. 3, and the brackets serve the same purpose throughout. Next the interference signal in the Twyman–Green interferometer is given by

$$S_c(x, t) = [1 + \gamma_1 a_1 \cos(\omega_m t + \theta_1)] \times \{S_{c1} + S_{c2} \cos[z_c \cos(\omega_m t + \theta_1) + \alpha(x)]\}, \tag{4}$$

where

$$z_c = 2\pi a_1 \beta_1 l/\lambda_0^2 \tag{5}$$

is modulation depth, l is optical path difference, and $\alpha(x)$ is phase distribution. S_{c1} and S_{c2} are the dc component and the amplitude of the ac component of the interference signal, respectively. The second term of the coefficient $[1 + \gamma_1 a_1 \cos(\omega_m t + \theta_1)]$ in Eq. (4) gives the intensity modulation and is identified as the source of the measurement error.

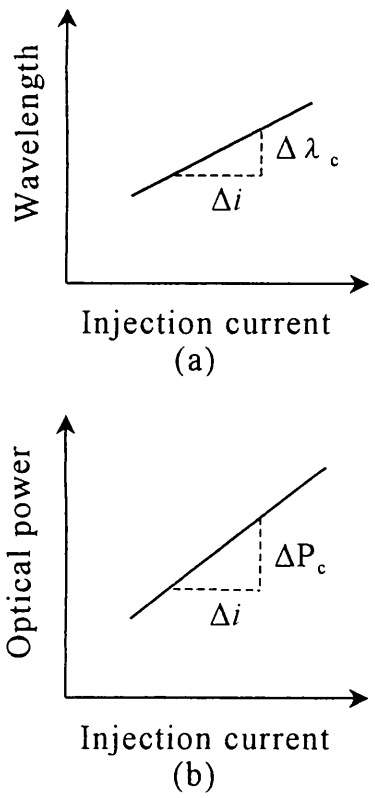

Fig. 2. Characteristics of LD's (a) wavelength tunability and (b)optical power change with injection current.

B. Photothermal Modulation

As stated above, and as shown in Fig. 3, wavelength and optical power vary according to temperature. Their coefficients are denoted by $\Delta\lambda_p/\Delta T$ and $\Delta P_p/\Delta T$ as shown in Figs. 3(a) and 3(b), respectively. The wavelength tunability with temperature is applicable

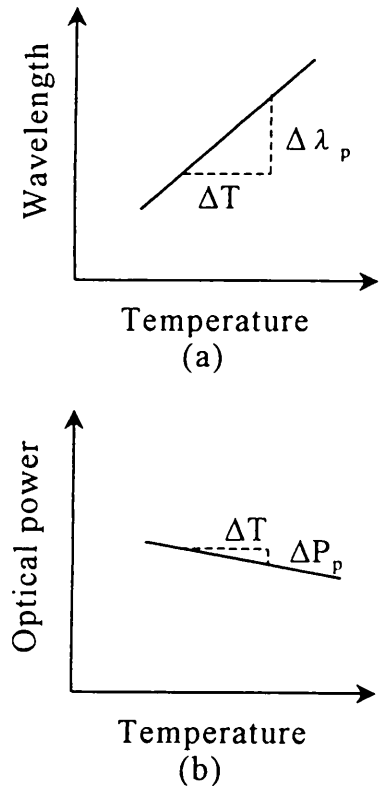

Fig. 3. Characteristics of LD's (a) wavelength tunability and (b) optical power change with temperature. $\Delta P_p/\Delta T$ is negative.

to the P modulation as well. In the P modulation shown in Fig. 1(b) we use intensity-modulated LD2 whereas LD1 is injected with dc bias current I_1 only. When both dc bias current I_2 and modulating current

$$i_2(t) = a_2 \cos(\omega_m t + \theta_2) \tag{6}$$

are injected into LD2, its optical power varies by

$$P_{c2}(t) = [\Delta P_{c2}/\Delta i_2] i_2(t), \tag{7}$$

according to the characteristic shown in Fig. 2(b). This intensity-modulated laser beam is fed into LD1 through the exit pupil, and it heats the laser chip in LD1. The temperature change influences the wavelength of LD1. Consequently the wavelength of LD1 in Fig. 1(b) varies by

$$\lambda_{p1}(t) = \left[\frac{\Delta\lambda_{p1}}{\Delta T_1}\right]\left[\frac{\Delta T_1}{\Delta P_{c2}}\right]\left[\frac{\Delta P_{c2}}{\Delta i_2}\right] i_2(t) \equiv \beta_2 i_2(t), \tag{8}$$

where β_2 is a modulating efficiency in the P modulation. $\Delta T_1/\Delta P_{c2}$, the conversion efficiency from optical power to temperature, depends on the optical setup and especially on the alignment of the optical axis. In the same way the optical power change in LD1 is represented by

$$P_{p1}(t) = \left[\frac{\Delta P_{p1}}{\Delta T_1}\right]\left[\frac{\Delta T_1}{\Delta P_{c2}}\right]\left[\frac{\Delta P_{c2}}{\Delta i_2}\right] i_2(t) \equiv \gamma_2 i_2(t), \tag{9}$$

where γ_2 is a coefficient of the optical power change in the P modulation and its sign is opposite to γ_1. The modulated interference signal is given by

$$S_p(x, t) = [1 + \gamma_2 a_2 \cos(\omega_m t + \theta_2)] \times \{S_{p1} + S_{p2} \cos[z_p \cos(\omega_m t + \theta_2) + \alpha(x)]\}, \tag{10}$$

where

$$z_p = 2\pi a_2 \beta_2 l/\lambda_0^2. \tag{11}$$

Although γ_2 is small compared with γ_1, the modulated interference signal still has a change in its amplitude. Compensation of this intensity modulation, however, is important when a precise measurement is called for.

C. Current and Photothermal Modulation

Note that the coefficients β_1 and β_2 share the same sign but those of γ_1 and γ_2 are opposite. When we employ C and P modulation simultaneously, the intensity modulation derived from the latter can be compensated by the former. Then the interference signal is given by

$$S_{cp}(x, t) = [1 + \gamma_1 a_1 \cos(\omega_m t + \theta_1) + \gamma_2 a_2 \cos(\omega_m t + \theta_2)] \times \{S_{cp1} + S_{cp2} \cos[z_{cp} \cos(\omega_m t + \theta_3) + \alpha(x)]\}, \tag{12}$$

where

$$z_{cp} = 2\pi(a_1\beta_1 + a_2\beta_2)l/\lambda_0^2. \tag{13}$$

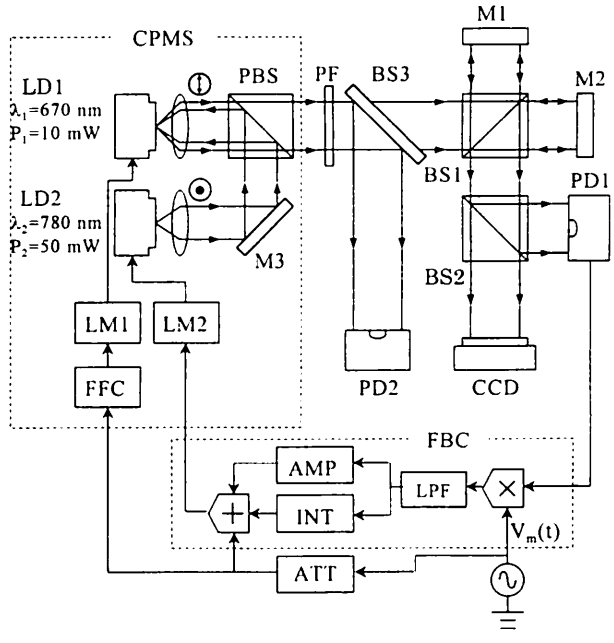

Fig. 4. Experimental setup of the *CP*-modulating system with a feedback control. CPMS, current and photothermal modulating system; FBC, feedback controller; LD1, laser for a light source; LD2, heating laser; PBS, polarizing beam splitter; BS, beam splitter; M, mirror; AMP, amplifier; INT, integrator; ATT, attenuator.

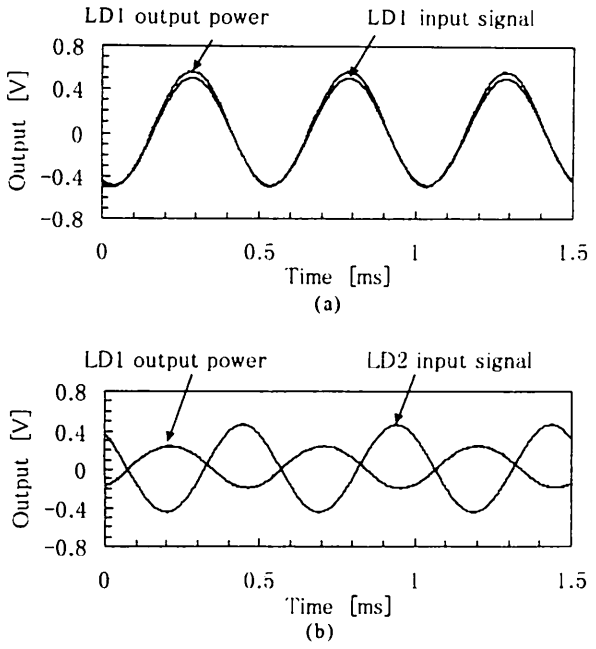

Fig. 5. Optical power changes in the LD with respect to the injection current (a) for LD1 and (b) for LD2.

If the conditions of $|\gamma_1 a_1| = |\gamma_2 a_2|$ and $\theta_1 = \theta_2$ hold, by adjustment of amplitude a_1 and phase θ_1 in the modulating or the compensating current $i_1(t)$, then intensity modulation is assumed to have no effect. Moreover, fortunately, Eq. (13) indicates that the modulation depth in *CP* modulation becomes larger than that in *P* modulation alone.

3. Experimental Setup

Our experimental setup is shown in Fig. 4. LD1 is a light source for the interferometer. The laser beam emitted from LD2 is injected into LD1 from its exit face. The central wavelengths and the maximum output powers of the LD's are shown in Fig. 4. LD modulators LM1 and LM2 generate the LD's driving currents that are correspond to the input voltages. Their gains are 22.9 and 62.6 mA/V, respectively. The optical path difference l is 60 mm. The polarizations of the LD's are perpendicular to each other to avoid the interference between LD1 and LD2. Undesired light radiated by LD2 is removed with a polarizing filter. Any changes in the output intensity of LD1 are monitored by photodetector 2 (PD2). Temporal changes in the interference signal are detected by PD1 and relayed to the feedback controller to eliminate external disturbance.[9] The sinusoidal signal $V_m(t)$ and the feedback signal are added and are injected into the heating laser LD2.

The modulating signal $V_m(t)$ is also transmitted to the feedforward controller to compensate for the intensity modulation in the interference signal. Amplitude a_1 and phase θ_1 of LD1's injection current are adjusted by the feedforward controller to satisfy the conditions described in Section 2. The spatial change of the interference signal is detected by the

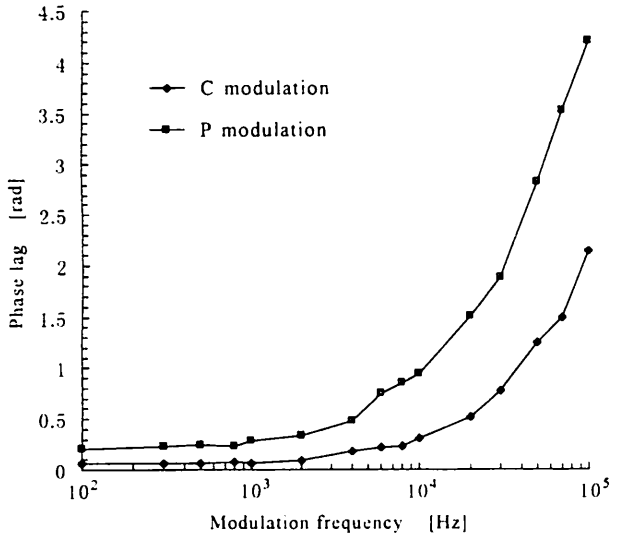

Fig. 6. Phase lags in the *C*- and the *P*-modulated interference signals with respect to the frequency of the injection current.

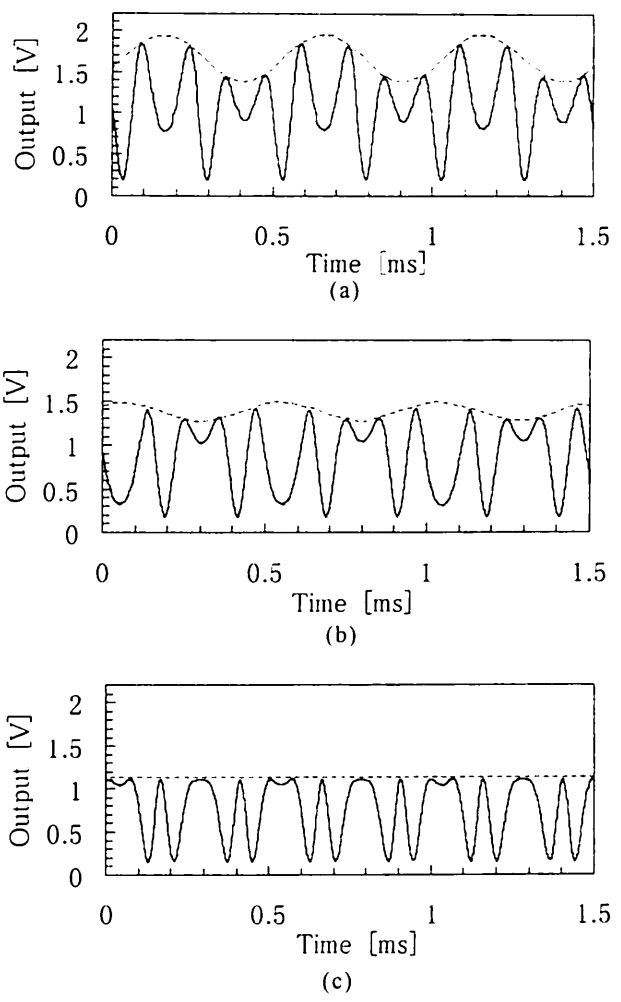

Fig. 7. Interference signals obtained by (a) *C* modulation, (b) *P* modulation, and (c) *CP* modulation. Modulation frequency is 2 kHz. Dashed curve, distortion introduced by the intensity modulation.

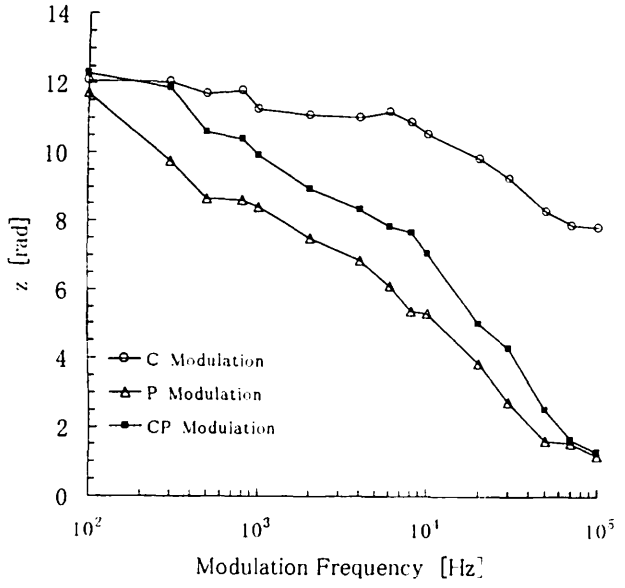

Fig. 8. Dependency of modulation depth z on modulation frequency.

one-dimensional CCD image sensor and is processed by a computer.

4. Experimental Results

A. Characteristics of the Modulating Methods

First, the characteristics of the *C* and the *P* modulation were examined in detail. Figure 5 shows the optical power changes detected by PD2 in the experimental setup, in which the LD1 is sinusoidally modulated with *C* or *P* modulation, respectively. The modulation frequency was 2 kHz. In the *C* modulation the output power of LD1 varies with injection current as shown in Fig. 5(a). In this figure the change has the same phase as the injection current. But in the *P* modulation shown in Fig. 5(b) the output power of LD1 is inversely proportional to the injection current of LD2. These two results can be explained by the LD's characteristics as shown in Figs. 2(b) and 3(b), respectively.

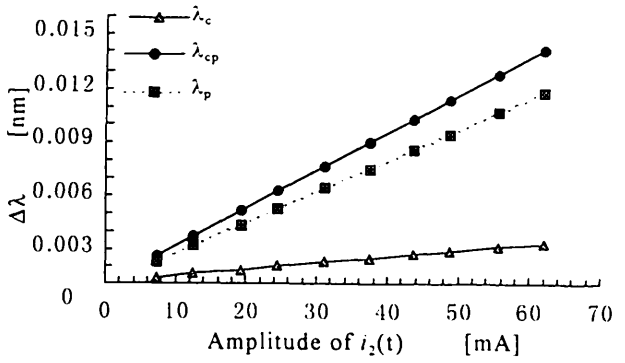

Fig. 9. Wavelength shift corresponding to amplitude of i_2(t). In the *CP* modulation, wavelength shifts by λ_p and λ_c with the *P* modulation and the *C* modulation, respectively. Total wavelength shift λ_{cp} becomes the sum of λ_p and λ_c in *CP* modulation.

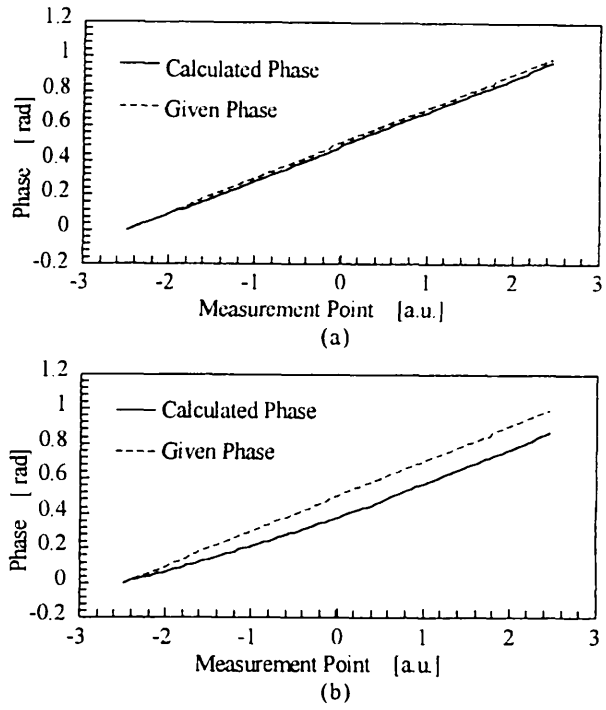

Fig. 10. Deviations of the phase extracted from the intensity-modulated interference signal with visibility of 100%. γ, the coefficient of the optical power changes, are (a) 0.1 and (b) 0.5.

Figure 5 shows that the phase of the output power is delayed slightly with respect to the injection current of LD2. We measured this phase lag by changing the frequency of the injection current. Results are shown in Fig. 6. The phase lag in the *P* modulation is larger than that in the *C* modulation. This shows that we have to apply appropriate phase delay to the compensating current in the *CP* modulation.

We measured the modulation efficiencies β_1 and β_2 denoted in Eqs. (2) and (8). The amplitudes of the modulating current were 0.8 and 21.5 mA in the *C* modulation and the *P* modulation, respectively, when the modulation depths z_c and z_p were set at $\pi/2$. Therefore β_1 and β_2 are calculated as 4.676×10^{-3} nm/mA and 1.740×10^{-4} nm/mA, respectively, by use of Eqs. (5) and (11). β_2 varies, of course, depending on the optical alignment; it is small compared with β_1.

Next we discuss the advantages of *CP* modulation as compared with the modulating methods mentioned above. Interference signals obtained by the three kinds of method are shown in Fig. 7. Figures 7(a) and 7(b) are obtained by means of *C* modulation and *P* modulation, respectively. The effect that intensity modulation exerts on the *P* modulation is much smaller than that in the *C* modulation. But it is difficult to make a precise measurement with this intensity-modulated interference signal. The trace obtained by the *CP* modulation is shown in Fig. 7(c). Modulating conditions on the *P* modulation in Fig. 7(c) are the same as those in Fig. 7(b). The effect of intensity modulation is completely eliminated in the *CP* modulation.

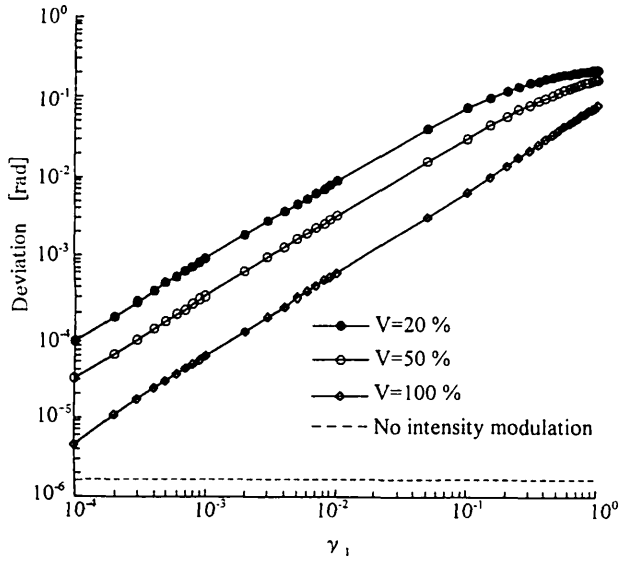

Fig. 11. Dependency of deviations on coefficient γ_1. Although the deviation reduces as the visibility increases, considerable error still remains.

Dependency of the modulation depth z on the modulating frequency is shown in Fig. 8. The cutoff frequency at the −3-dB level of the modulation depth z reaches 50 kHz in the C modulation whereas that in P modulation is 1 kHz. It is, however, improved to 4 kHz in the CP modulation, as explained in Eq. (13).

Moreover, wavelength shift in the CP modulation was measured. The wavelength shift shown in Fig. 9 is calculated with the interference signal that is modulated by a sinusoidal current. Data plotted by squares are wavelength shift $\Delta\lambda_p$ corresponding to the amplitude of modulating current $i_2(t)$. At this time, intensity modulation is simultaneously compensated by the modulating current $i_1(t)$ generated in the feedforward controller. Then the wavelength is varied by $i_1(t)$ as well. Wavelength shift is plotted with triangles as $\Delta\lambda_c$ in Fig. 9. Exact wavelength shift in LD1 is then measured and plotted with circles. We can find that the wavelength shift $\Delta\lambda_{cp}$ in CP modulation is given as the sum of $\Delta\lambda_p$ and $\Delta\lambda_c$.

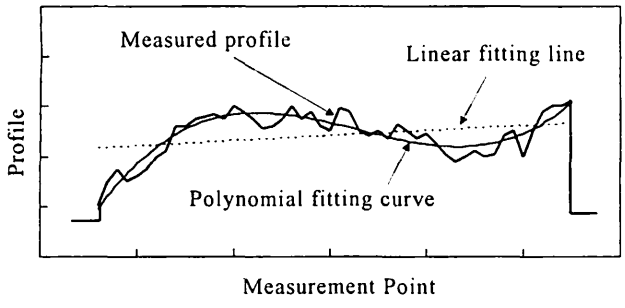

Fig. 12. Schematic of calculation method for σ, which is denoted by the rms value of the difference between the linear fitting line and the polynomial fitting curve of degree three.

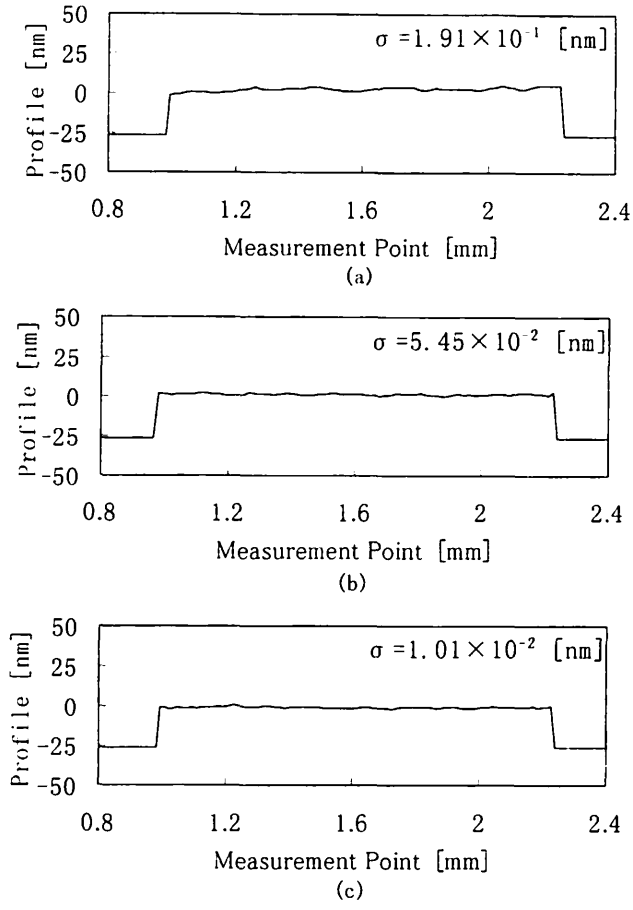

Fig. 13. Surface profile of flat mirror measured with (a) C modulation, (b) P modulation, and (c) CP modulation. σ's are the differences between the fitting line and the fitting curve, and they indicate that CP modulation is useful for reducing the deviation caused by the intensity modulation.

B. Application for the Surface-Profile Measurement

First, by means of simulation, we estimated the measurement error that is introduced by the intensity modulation. In this case the error appears as a nonlinear distortion in the measurement results. In the simulation the interference signal was generated with Eq. (4) for a linear phase distribution $\alpha(x)$. Then we extracted $\alpha(x)$ from the interference signal by using the bucket method. Simulations were made by variation of the visibility S_{c2}/S_{c1} and γ_1, the coefficient of the optical power change. Major results with a visibility of 100% are shown schematically in Fig. 10, in which (a) and (b) are obtained at γ_1 = 0.1 and 0.5, respectively. As γ_1 increases, deviation in the extracted phase becomes large even if the interference signal has a maximum visibility of 100%. Deviations, which are denoted by the rms error with respect to the given phase, were calculated for various γ_1 by changing of the visibility V. Results are plotted in Fig.11. Although the deviation reduces as the visibility increases, considerable error still remains.

Next we measured the surface profile of a flat mirror by using a one-dimensional CCD image sensor

and estimated the deviations influenced by the intensity modulation. To execute numerical comparison in the deviations, we calculate the first-order approximate line and the third-order approximate curve by using the measured data. The deviation σ is denoted by the rms value of the difference between the fitting line and the curve as shown in Fig. 12. Results obtained by the *C*, *P*, and *CP* modulations are shown in Figs. 13(a), 13(b), and 13(c), respectively. Then the deviations were calculated as 1.91×10^{-1}, 5.45×10^{-2}, and 1.01×10^{-2} for the *C*, *P*, and *CP* modulations, respectively. It was confirmed that the *CP* modulation is useful for generating the ideal interference signal, and it enables us to reduce measurement error caused by the intensity modulation.

5. Conclusions

We have proposed a mechanically simple yet highly accurate modulating technique that uses both current modulation and photothermal modulation, simultaneously, to remove undesirable intensity modulation from the interference signal. We have formularized each modulating method, including conventional current modulation. The current (C) and the photothermal (P) modulations use the difference between the dependencies of the LD's output power on the injection current and on the temperature. We have shown these characteristics in the experiment. The interference signals modulated by three kinds of method have been observed and compared. Those observations enable us to confirm the advantage of the current and photothermal (CP) modulation that is free from intensity modulation. This technique is simple, easy to realize, and useful for generating a purely phase-modulated laser beam.

References

1. J. Chen, Y. Ishii, and K. Murata, "Heterodyne interferometry with a frequency-modulated laser diode," Appl. Opt. **27,** 124–128 (1988).
2. Y. Ishii, J. Chen, and K. Murata, "Digital phase-measuring interferometry with a tunable laser diode," Opt. Lett. **12,** 233–235 (1987).
3. K. Tatsuno and Y. Tsunoda, "Diode laser direct modulation heterodyne interferometer," Appl. Opt. **26,** 37–40 (1987).
4. P. Hariharan, "Phase-stepping interferometry with laser diodes: effect of changes in laser power with output wavelength," Appl. Opt. **28,** 27–29 (1989).
5. T. Suzuki, O. Sasaki, K. Higuchi, and T. Maruyama, "Real-time displacement measurement in sinusoidal phase modulating interferometry," Appl. Opt. **28,** 5270–5274 (1989).
6. R. Onodera and Y. Ishii, "Two-wavelength phase-shifting interferometry insensitive to the intensity modulation of dual laser diodes," Appl. Opt. **33,** 5052–5061 (1994).
7. C. M. Kiimcak and J. C. Camparo, "Photothermal wavelength modulation of a diode laser," J. Opt. Soc. Am. B **5,** 211–214 (1988).
8. R. D. Esman and D. L. Rode, "Semiconductor-laser thermal time constant," J. Appl. Phys. **59,** 407–409 (1986).
9. O. Sasaki, K. Takahashi, and T. Suzuki, "Sinusoidal phase modulating laser diode interferometer with a feedback control system to eliminate external disturbance," Opt. Eng. **29,** 1511–1515 (1990).